Peculiar Magnetic Behavior of the $TbCu_3Mn_4O_{12}$ Complex Perovskite

J. Sánchez-Benítez,*,† J. A. Alonso,† A. de Andrés,† M. J. Martínez-Lope,† J. L. Martínez,† and A. Muñoz‡

Instituto de Ciencia de Materiales de Madrid, Consejo Superior de Investigaciones Científicas, Cantoblanco, E-28049 Madrid, Spain, and Departamento de Física Aplicada, EPS, Universidad Carlos III, Avenida Universidad 30, E-28911, Leganés-Madrid, Spain

Received June 13, 2005. Revised Manuscript Received August 5, 2005

$TbCu_3Mn_4O_{12}$ perovskite has been prepared in polycrystalline form under moderate pressure conditions of 2 GPa, in the presence of $KClO_4$ as oxidizing agent. This material has been studied by X-ray and neutron powder diffraction (XRD and NPD) and magnetotransport measurements. The crystal structure is cubic, space group $Im\bar{3}$ (No. 204), with **a** = 7.2668(1) Å at room temperature (RT). This compound presents a ABO_3 perovskite superstructure, where the A positions are occupied by Tb and Cu, ordered in a 1:3 arrangement, giving rise to the body centering of the unit cell. At the B positions, Mn adopts a mixed oxidation state of 3.75+; MnO_6 octahedra are considerably tilted by 19°, due to the relatively small size of the A-type cations. $TbCu_3Mn_4O_{12}$ is ferrimagnetic below $T_C = 395$ K: the magnetic structure, studied by NPD, reveals that Mn and Cu spins are ordered below T_C in an antiparallel arrangement. Additionally, below 100 K the Tb magnetic moments also participate in the magnetic structure, becoming antiferromagnetically coupled to Mn spins. This arrangement can be broken under the presence of an external magnetic field, inducing a turnover of the Tb magnetic moments, which then become parallel to the Mn moments. The mixed valence state created at the Mn sublattice is responsible for the observed metallic behavior; a negative magnetoresistance of 25% is achieved at 5 K for $H = 9$ T.

Introduction

Considerable attention has been paid to manganese perovskites owing to their colossal magnetoresistance (CMR) and other novel properties.[1,2] Generally speaking, the CMR effect of polycrystalline ceramics and films falls into two classes, namely, the intrinsic and extrinsic magnetoresistance (MR). The former is referred to intragrain MR, which has a maximum near the ferromagnetic transition temperature, T_C. The latter is intergrain MR observed over a wider temperature range below T_C and is characteristic of a large low-field MR, which is attributed to spin-polarized tunneling or spin-dependent scattering at grain boundaries and other interfaces in polycrystalline samples. Because a large low-field MR is highly desirable from the viewpoint of the practical application, how to increase the extrinsic MR effect of polycrystalline samples in low magnetic fields has become one of the important investigation subjects, not only in the more conventional hole-doped $RMnO_3$ (R = rare earths) perovskites, but in other more innovative and complex perovskite systems.

Recently, a "new" system has attracted the attention of the CMR community: the complex perovskite $CaCu_3Mn_4O_{12}$.[3−6] This ferromagnetic oxide ($T_C = 355$ K) shows good low-field response, as large as 40% at 20 K, and this response does not show the strong temperature-dependent decay characteristic of other perovskite-based systems. This is appealing since, for practical application, significant temperature stability is required around room temperature.[7,8] $CaCu_3Mn_4O_{12}$ had already been described in the 1970s, when the preparation and crystal structure of some related phases ($A'A_3B_4O_{12}$ family) was reported.[9−11] The crystal structure of this compound has the originality of containing Cu^{2+} (or other Jahn−Teller transition metal cations) at the A positions of the ABO_3 perovskite. The crystal symmetry is cubic (space group $Im\bar{3}$) with a doubling of the ideal perovskite cell. The superstructure is due to the 1:3 ordering of the A′ and A (Jahn−Teller) ions and the distortion of the oxygen sublattice, which leads to a three-dimensional network of strongly tilted BO_6 octahedra sharing corners.[12] The B−O−B angle is ∼142° instead of 180°, as

* To whom correspondence should be addressed.
† Consejo Superior de Investigaciones Científicas.
‡ Universidad Carlos III.

(1) Ramirez, A. P. *J. Phys: Condens. Matter* **1997**, *9*, 8171.
(2) Rao, C. N. R., Raveau, B., Eds. *Colossal magnetoresistance and other related properties in 3d oxides*; World Scientific: Singapore, 1998.
(3) Zeng, Z.; Greenblatt, M.; Subramanian, M. A.; Croft, M. *Phys. Rev. Lett.* **1999**, *82*, 3164.
(4) Wu, H.; Zheng, Q.; Gong, X. *Phys. Rev. B* **2000**, *61*, 5217.
(5) Weht, R.; Pickett, W. E. *Phys. Rev. B* **2001**, *65*, 14415.
(6) Troyanchuk, I. O.; Lobanovsky, L. S.; Kasper, N. V.; Hervieu, M.; Maignan, A.; Michel, C.; Szymczak, H.; Szewczyk, A. *Phys. Rev. B* **1998**, *58*, 14903.
(7) Sánchez-Benítez, J.; Alonso, J. A.; Martínez-Lope, M. J.; Casais, M. T.; Martínez, J. L.; de Andrés, A.; Fernández-Díaz, M. T. *Chem. Mater.* **2003**, *15*, 2193.
(8) Alonso, J. A.; Sánchez-Benítez, J.; de Andrés, A.; Martínez-Lope, M. J.; Casais, M. T.; Martínez, J. L. *Appl. Phys. Lett.* **2003**, *83*, 2623.
(9) Chenavas, J.; Joubert, J. C.; Marezio, M.; Bochu, B. *J. Solid State Chem.* **1975**, *14*, 25.
(10) Bochu, B.; Chenavas, J.; Joubert, J. C.; Marezio, M. *J. Solid State Chem.* **1974**, *11*, 88.
(11) Marezio, M.; Dernier, P. D.; Chenavas, J.; Joubert, J. C. *J. Solid State Chem.* **1973**, *6*, 16.
(12) Deschizeaux, M. N.; Joubert, J. C.; Vegas, A.; Collomb, A.; Chenavas, J.; Marezio, M. *J. Solid State Chem.* **1976**, *19*, 45.

10.1021/cm051265l CCC: $30.25
Published on Web 09/10/2005

in the ideal perovskite structure. This distortion creates two different polyhedra at the A′/A site: a slightly distorted 12 oxygen-coordinated A′ site and a grossly distorted icosahedron at the A site. There are three sets of A−O distances at ∼1.9, 2.8, and 3.2 Å, each forming an approximately square-planar coordination for A Jahn−Teller cations.

$CaCu_3Mn_4O_{12}$, and other compounds of the $A'A_3B_4O_{12}$ family, have been prepared under high pressure (7 GPa), necessary to stabilize the small A cations in the 12-fold coordinated positions of the perovskite. Recently, we have been able to synthesize polycrystalline samples of $CaCu_3Mn_4O_{12}$ derivatives at moderate pressures of 2 GPa, starting from very reactive precursors obtained by wet-chemistry procedures, in the presence of $KClO_4$ as in situ oxidizing agent.[7] This alternative preparation procedure allowed us to obtain well-crystallized samples, suitable to perform an accurate neutron diffraction study of both structure and magnetism, and a complete characterization of the magnetic and magnetotransport properties.

In this system, Ca cations can be replaced by rare earths in the $RCu_3Mn_4O_{12}$ (R = rare earths) series, implying an electron doping effect that affects the magnetic and transport properties, as demonstrated for R = La, Ce, Nd, and Th.[8,13] In the case of R = La[8] we have described an excellent low-field MR magnitude at RT, comparable to the best values known for bulk magnetoresistance materials at RT.

Magnetotransport properties of R = Tb compound was described by Troyanchuk et al.[6,14] In this paper we present a description of the chemical preparation of this complex perovskite under moderate pressure conditions, and we report on a structural and magnetic study of $TbCu_3Mn_4O_{12}$ by neutron powder diffraction, complementary to magnetic measurements. We show that, besides the expected ferrimagnetic order of Mn and Cu ions below T_C, the rare-earth magnetic moments also play an important role at low temperatures, leading to a peculiar magnetic behavior, which has been studied under very high fields up to 16 T.

Experimental Section

The elaboration of $TbCu_3Mn_4O_{12}$ required the previous preparation of very reactive precursors, obtained by wet-chemistry techniques. A mixture of Tb_4O_7, $Cu(NO_3)_2{\cdot}3H_2O$, and $MnCO_3$ was dissolved in citric acid; the solution was slowly evaporated, leading to an organic resin which was dried at 120 °C and slowly decomposed at temperatures up to 600 °C. The sample was then heated at 800 °C for 2 h in order to eliminate all the organic materials and nitrates. This precursor was thoroughly ground with $KClO_4$ (30% in weight), put into a gold capsule (8 mm diameter, 10 mm length), sealed, and placed in a cylindrical graphite heater. The reaction was carried out in a piston-cylinder press (Rockland Research Co.), at a pressure of 2 GPa at 1000 °C for 60 min. Then the material was quenched to room temperature and the pressure was subsequently released. The raw product, obtained as a dense, homogeneous pellet, was ground to perform the structural and magnetic characterization. The ground product was washed in a dilute HNO_3 aqueous solution, to dissolve KCl coming from the decomposition of $KClO_4$ and to eliminate small amounts of unreacted CuO; then the powder sample was dried in air at 150 °C for 1 h.

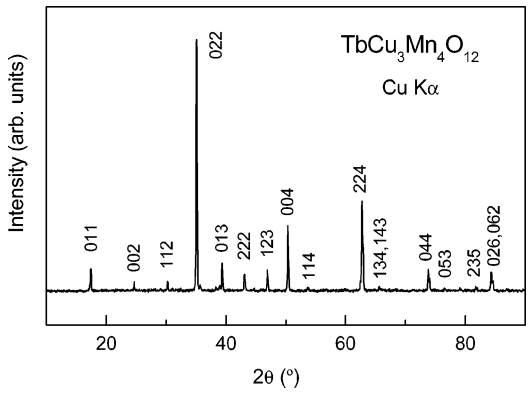

Figure 1. XRD pattern for $TbCu_3Mn_4O_{12}$ indexed in a cubic unit cell with **a** = 7.2668(8) Å.

The product was initially characterized by laboratory XRD (Cu Kα, λ = 1.5406 Å) for phase identification and to assess phase purity. For the structural refinements, NPD patterns were collected at room temperature and 2 K at the high resolution D2B neutron diffractometer of ILL-Grenoble. Despite the relatively small amount of sample available (about 1 g), a good quality pattern could be collected with the high-flux mode and a counting time of 4 h for each pattern. A wavelength of 1.594 Å was selected from a Ge monochromator. Low-temperature medium-resolution NPD patterns were collected at the high-flux D20 diffractometer (2.42 Å), to follow the thermal evolution of the ferromagnetic component. The sample was placed in a standard orange cryostat and cooled to 2.5 K; then sequential NPD diagrams were collected during the heating run, at 0.8 K min^{-1}, in the 2.5−285 K temperature range, with a counting time of 10 min per diagram. All the patterns were refined by the Rietveld method, using the FULLPROF refinement program.[15] A pseudo-Voigt function was chosen to generate the line shape of the diffraction peaks. No regions were excluded in the refinement. In the final run the following parameters were refined from the high-resolution D2B data: scale factor, background coefficients, zero-point error, unit-cell parameters, pseudo-Voigt corrected for asymmetry parameters, positional coordinates, isotropic thermal factors, and magnitude of the Cu, Mn, and Tb magnetic moments. The coherent scattering lengths for Tb, Cu, Mn, and O were 7.34, 7.718, −3.73, and 5.805 fm, respectively. The magnetic form factors considered for Cu, Mn, and Tb cations were determined with the coefficients taken from the International Tables of Crystallography.

The dc magnetic susceptibility was measured on a powdered sample with a commercial SQUID magnetometer from Quantum Design, in the temperature range 2−800 K. The magnetization vs magnetic field measurements at 2, 20, and 100 K were performed up to 16 T in a Physical Properties Measurement System (PPMS) also from Quantum Design.

Results

$TbCu_3Mn_4O_{12}$ was obtained as a black, well-crystallized powder. The laboratory XRD diagram is shown in Figure 1. The pattern is characteristic of a cubic perovskite showing sharp, well-defined superstructure reflections due to the 1:3 ordering of Tb and Cu cations. The observed unit-cell parameter, of 7.2668(1) Å, agrees with that described

(13) Sánchez-Benítez, J.; Alonso, J. A.; de Andrés, A.; Martínez-Lope, M. J.; Casais, M. T.; Martínez, J. L. *J. Magn. Magn. Mater.* **2004**, *272*, e1407.
(14) Troyanchuk, I. O.; Khalyavin, D. D.; Hervieu, M.; Maignan, A.; Michel, C.; Petrowski, K. *Phys. Status Solidi A* **1998**, *169*, R1.
(15) Rodríguez-Carvajal, J. *Physica B* (Amsterdam) **1993**, *192*, 55.

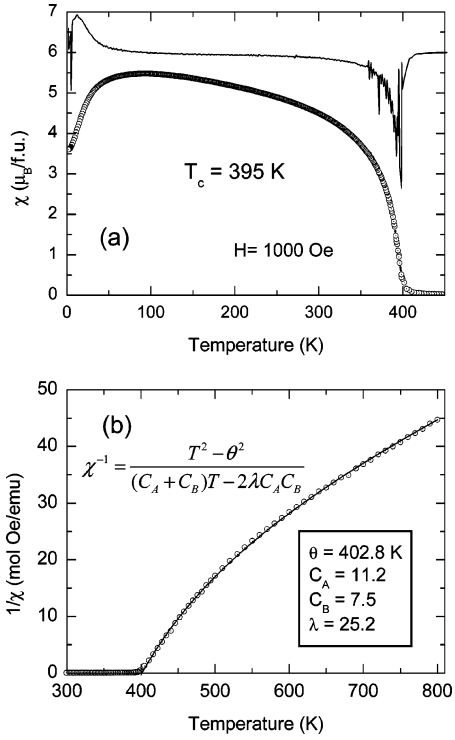

Figure 2. Temperature dependence of the (a) dc magnetic susceptibility (with its derivative) and (b) reciprocal susceptibility for $TbCu_3Mn_4O_{12}$. C_A and C_B are expressed in emu·K/mol·Oe units.

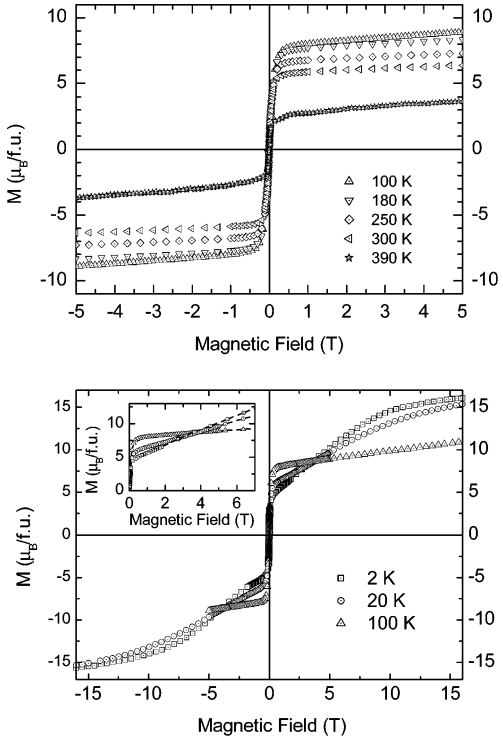

Figure 3. Upper panel: magnetization vs magnetic field isotherms for $TbCu_3Mn_4O_{12}$ at different temperatures $T \geq 100$ K from −5 to 5 T. Lower panel: magnetization at some selected temperatures $T \leq 100$ K between −16 and 16 T. The inset is a close-up of the low-field region.

elsewhere, of 7.258(1).[6] No impurity phases were detected from either XRD or NPD data. This perovskite has been obtained by the total substitution of Ca by Tb in the parent compound $CaCu_3Mn_4O_{12}$. Owing to the oxidizing preparation conditions, Tb could adopt either a trivalent or tetravalent state. The change of Ca^{2+} by $Tb^{3+/4+}$ implies that Mn^{4+} at B site is partially reduced to Mn^{3+} to preserve the charge neutrality. This point will be subsequently discussed in light of the structural results.

Magnetic Data. The magnetization vs temperature data (Figure 2a) shows below 400 K a spontaneous increase of the susceptibility, characteristic of a ferrimagnetic ordering. It is well-established for the $CaCu_3Mn_4O_{12}$ system[7] that this effect corresponds to the antiferromagnetic coupling of the Cu and Mn magnetic sublattices. Additionally, at low temperatures the magnetization decreases remarkably, suggesting the ordering of the Tb magnetic sublattice. The inflection point in the magnetization, labeled as Curie temperature (T_C), is placed at 395 K. This T_C is somewhat higher than that reported by Troyanchuk et al.[6] Above T_C, the reciprocal susceptibility data (Figure 2b) shows a progressive change of slope, which diminishes as temperature increases. This behavior of the reciprocal susceptibility is a typical feature of ferrimagnetic compounds.

The data nicely fit the formula $\chi^{-1} = (T^2 - \theta^2)/((C_A + C_B)T - 2\lambda C_A C_B)$ that represent the reciprocal susceptibility of the paramagnetic phase of a ferrimagnetic compound,[16] where A and B stand for the two sublattices that experience antiferromagnetic coupling below the ordering temperature. The fit to the total paramagnetic range (400−800 K) gives the C_A and C_B Curie constants indicated in Figure 2b, from which we obtain the effective paramagnetic moments of 9.5 μ_B/f.u. and 7.78 μ_B/f.u. for both A (Cu^{2+} + Tb^{3+}) and B ($Mn^{3+/4+}$) sublattices, very close to the expected 9.96 μ_B/f.u. and 8.3 μ_B/f.u. obtained considering the standard values of $\mu_{para} = 9.5$, 1.73, 4.9, and 3.87 μ_B for Tb^{3+}, Cu^{2+}, Mn^{3+}, and Mn^{4+}, respectively. The obtained Weiss constant, $\theta =$ 402.8 K, is significantly close to the Curie temperature and indicates the predominance of ferromagnetic interactions in the system.

Figure 3 shows the magnetization vs magnetic field data at different temperatures. Down to 100 K (upper panel of Figure 3) the shape of the curves is characteristic of a ferrimagnet with a saturation magnetization corresponding to the antiparallel alignment between Mn and Cu spins. Below 100 K (lower panel), low-field magnetization data reach smaller M values for lower temperatures that gradually increase with the external applied field evidenced in the measurements performed up to 16 T. This is in good agreement with the susceptibility curve in Figure 2, where a progressive decrease is observed between 100 and 2 K. The evolution of the magnetization isotherms features a "crossover" at around 4 T; above this value the magnetization is larger at 2 K than 100 K. At 20 and 2 K the magnetization does not reach a saturation value, at least up to 16 T. This behavior can be understood in the light of the low-temperature magnetic structure, described below.

Magnetotransport Measurements. The transport properties of $TbCu_3Mn_4O_{12}$ are illustrated in Figure 4. The resistivity at $H = 0$ displays a metallic behavior in all of the temperature range $2 < T < 400$ K. It is worth mentioning that the observed value for $\rho(T{=}300\text{K}, H{=}0)$, of 0.03 Ω·

(16) Kittel, C. *Introduction to Solid State Physics*; John Wiley: New York, 1993.

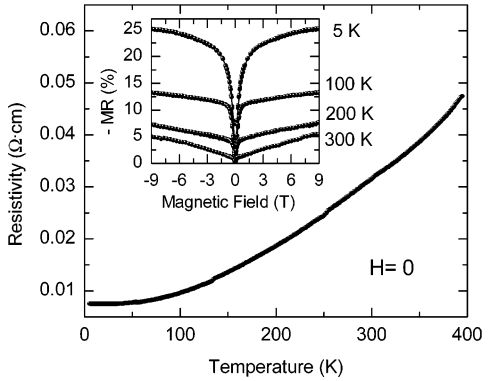

Figure 4. Resistivity vs temperature curves at $H = 0$ for $TbCu_3Mn_4O_{12}$. Inset: magnetoresistance (MR) isotherms. MR is defined as $100 \times [R(H) - R(0)]/R(0)$.

cm, is considerably smaller than that described for the parent $CaCu_3Mn_4O_{12}$ compound, of $\sim 1.8 \times 10^3$ Ω·cm.[5] The metallic behavior and the low resistivity can be explained by the partial filling of the e_g Mn band of the Mn located at B site.[17] Regarding the changes in $\rho(T)$ under a magnetic field, we define $MR(H) = 100 \times [R(H) - R(0)]/R(0)$. The inset of Figure 4 illustrates some selected isotherms for external applied fields $-9 < H < 9$ T. A maximum negative MR of 25% is achieved at 5 K for $H = 9$ T; MR is still significant at RT, displaying values close to 5% for $H = 9$T.

Structural Refinement at RT. The structural refinement from RT high-resolution NPD data was performed in the $Im\bar{3}$ (No. 204) space group, with a unit-cell parameter related to $\mathbf{a}_0$ (ideal cubic perovskite, $\mathbf{a}_0 \sim 3.8$ Å) as $\mathbf{a} \sim 2a_0$, using the parent $CaCu_3Mn_4O_{12}$ structure as the starting model, with Tb atoms at 2a (0,0,0) positions, Cu at 6b (0, $^1/_2$, $^1/_2$) positions, Mn at 8c ($^1/_4$,$^1/_4$,$^1/_4$), and O at 24g (0,*y*,*z*) sites. A good fit ($R_I \approx 4.22\%$) was obtained for this preliminary model. As a second step, the introduction of Mn atoms at random at 6b positions together with Cu was tried since Mn^{3+} is a Jahn−Teller cation suitable to occupy this crystallographic site, and the complementary occupancy factors were refined, constrained to a full occupancy. Nevertheless, Mn atoms were rejected from this position. After this step, the magnetic phase contribution was included as a second phase since this compound is magnetically ordered already at RT ($T_C = 395$ K), as shown from the magnetic measurements (Figure 2). We have modeled a perfect ferrimagnetic ordering between the magnetic moments at 6b and 8c positions, directed along the **c** axis; this model corresponds to a perfect collinear arrangement of Cu and Mn spins. After this refinement the quality of the fit was improved, reaching a discrepancy factor of $R_I = 3.49\%$. The magnetic phase had a discrepancy factor of 6.95%, yielding ordered magnetic moments of 1.77(6) μ_B and −0.27(7) μ_B for Mn and Cu sites, respectively. The subsequent refinement of the occupancy factor for oxygen positions gave no significant deviation from the full stoichiometry. The quality of the fit after the final refinement is illustrated in Figure 5a. The crystallographic formula for this material was confirmed to be $Tb[Cu_3]_{6b}[Mn_4]_{8c}O_{12}$. Table 1 lists the

(17) Sánchez-Benítez, J.; Prieto, C.; de Andrés, A.; Alonso, J. A.; Martínez-Lope, M. J.; Casais, M. T. *Phys. Rev. B* **2004**, *70*, 24419.

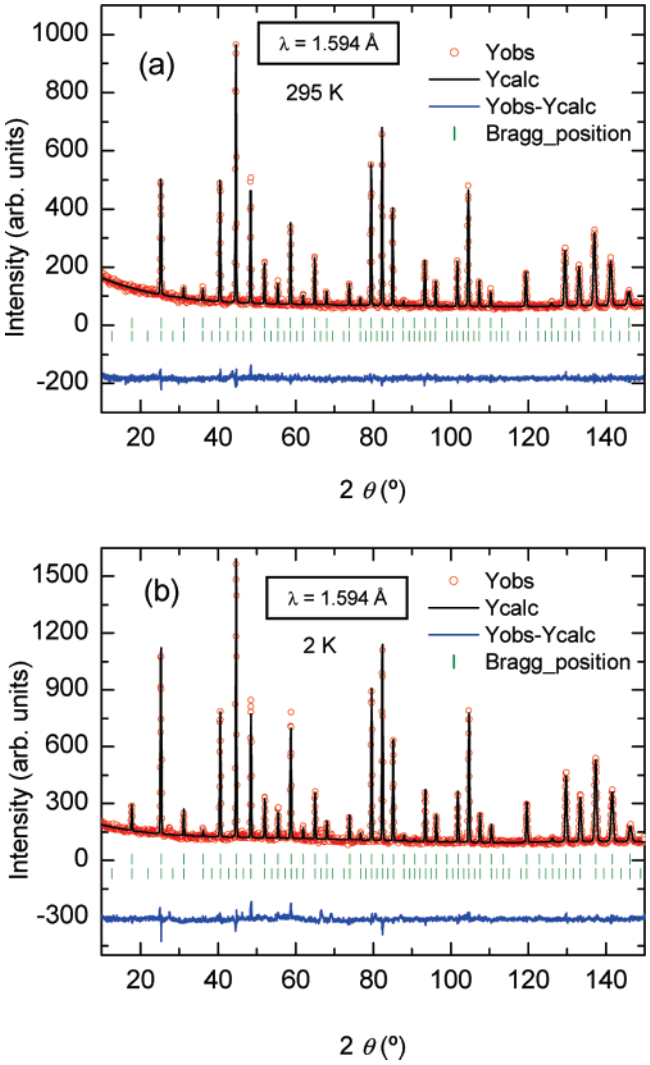

Figure 5. Observed (circles), calculated (full line), and difference (bottom) NPD Rietveld profiles for $TbCu_3Mn_4O_{12}$ at 295 K (a) and 2 K (b), collected at the high-resolution D2B-ILL diffractometer. The second row of tick marks corresponds, in both spectra, to the magnetic structure.

relevant parameters after the refinement from NPD data. Table 2 contains the main bond distances and angles.

Magnetic Structure Evolution. Figure 6 shows the thermal evolution of the NPD patterns of $TbCu_3Mn_4O_{12}$ in the 2.5−285 K temperature range, collected in the high-flux D20 diffractometer ($\lambda = 2.42$ Å). The variation of the integrated intensities of several selected reflections is shown in Figure 7.

There is a considerable magnetic contribution to the scattering on the low-angle Bragg reflections, for instance, on the [200] Bragg position, which smoothly increases below RT. This contribution is characteristic of a ferromagnetic or ferrimagnetic ordering, in which the magnetically ordered unit cell coincides with the crystallographic one. Additionally, there is a magnetic contribution on the [110] Bragg position, allowed by the symmetry of the $Im\bar{3}$ body-centered unit cell, at $2\theta \approx 28°$, the intensity of which drastically increases below 100 K. This additional contribution is also present in some higher angle reflections such as [211]. Finally, some peaks show a decrease of the integrated intensity, such as [220]. Two temperature regions have been distinguished concerning the magnetic structures which are

Table 1. Unit-Cell, Positional, Thermal Parameters and Ordered Magnetic Moments for $TbCu_3Mn_4O_{12}$ in Cubic $Im\bar{3}$ (No. 204) Space Group, $Z = 2$, from NPD Data at 295 and 2 K; Reliability Factors for Both Patterns Are Also Given

		295 K	2 K
a (Å)		7.2668(1)	7.2587(1)
V (Å^3)		383.725(8)	382.447(8)
Tb	2a (0 0 0)		
B (Å^2)		0.16(8)	0.15(8)
magn. mom. (μ_B)		0.0	−5.07(7)
Cu	6b (0 $^1/_2$ $^1/_2$)		
B (Å^2)		0.63(4)	0.39(4)
magn. mom. (μ_B)		−0.27(7)	−0.75(6)
Mn	8c ($^1/_4$ $^1/_4$ $^1/_4$)		
B (Å^2)		0.52(5)	0.31(5)
magn. mom. (μ_B)		1.77(6)	2.59(7)
O	24g (0 y z)		
y		0.2994(2)	0.2986(3)
z		0.1790(2)	0.1782(3)
B (Å^2)		0.48(2)	0.24(3)
reliability factors			
χ^2		1.20	2.00
R_p (%)		4.40	5.09
R_{wp} (%)		5.65	6.61
R_{exp} (%)		5.16	4.68
R_{mag} (%)		6.95	9.21
R_I (%)		3.49	6.36

Table 2. Main Bond Distances (Å) and Selected Angles (deg) for $TbCu_3Mn_4O_{12}$ Determined from NPD Data at 295 and 2 K

	295 K	2 K
TbO_{12} Polyhedra		
Tb−O (×12)	2.535(2)	2.524(2)
CuO_{12} Polyhedra		
Cu−O (×4)	2.7509(8)	2.7553(9)
Cu−O (×4)	3.190(1)	3.187(1)
Cu−O (×4)	1.954(2)	1.952(2)
O−Cu−O[a]	94.00(6)	97.0(1)
O−Cu−O[a]	86.00(3)	83.0(1)
MnO_6 Octahedra		
Mn−O (×6)	1.922(1)	1.921(1)
O−Mn−O	88.44(7)	88.1(1)
O−Mn−O	91.56(9)	91.9(1)
Cu−O−Mn	108.54(5)	108.51(5)
Mn−O−Mn	141.83(2)	141.75(2)

[a] For Cu−O short distances, within CuO_4 square units.

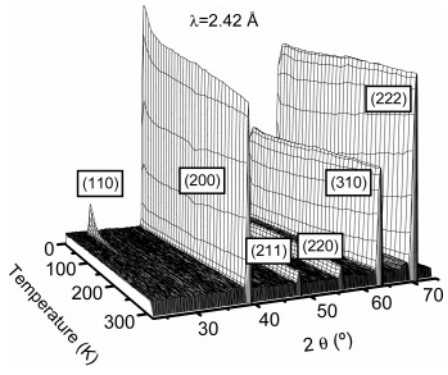

Figure 6. Thermal evolution of the low-angle region of the NPD patterns of $TbCu_3Mn_4O_{12}$ collected at the D20-ILL diffractometer.

schematized in Figure 8. In the temperature interval $100 < T <$ RT we have considered a perfect ferrimagnetic collinear arrangement of the Mn and Cu magnetic moments, as described in the precedent heading (Figure 8a). Below 100 K, Tb magnetic moments undergo long-range magnetic ordering. The magnetic intensities can be explained in a model where Tb magnetic moments are antiferromagnetically coupled with Mn spins, according to the scheme depicted in Figure 8b. It is important to underline that, although neutron powder diffraction techniques do not allow the determination of the absolute orientation of the magnetic moments in a cubic structure, it is indeed possible to determine the relative orientation of the moments of the different magnetic substructures. In this case we have considered that the first set of Mn moments at 8c positions is parallel to the **c**-axis, and then refined the orientation and magnitude of the Cu and Tb moments at 6b with respect to this reference.

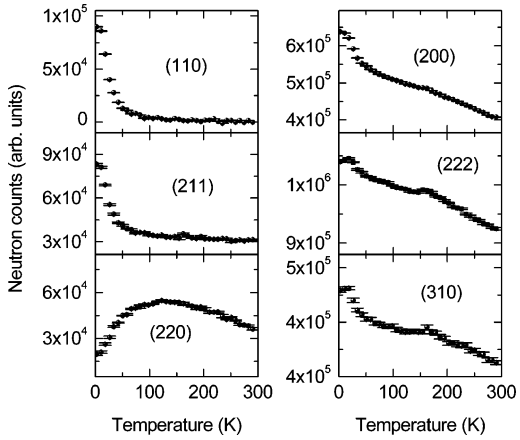

Figure 7. Thermal evolution of the integrated intensities of some selected NPD reflections of $TbCu_3Mn_4O_{12}$.

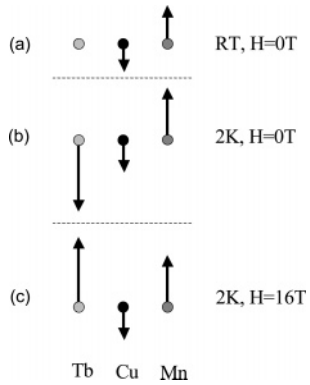

Figure 8. Schematic diagram showing the relative ordering of the magnetic moments of Tb, Cu, and Mn magnetic atoms observed by NPD at 295 K (a) and 2 K (b). It also shows the magnetic structure rearrangement upon application of an external magnetic field of 16 T at 2 K, obtained from the magnetization data (c).

The evolution of the magnitude of the different magnetic moments has been analyzed in a sequential refinement from NPD data, and it is displayed in Figure 9a. Mn and Cu moments, already ordered at RT, progressively increase in absolute value as temperature decreases. Tb ordered moment exhibits measurable values below 75 K, reaching $-5\ \mu_B$ at the lowest temperatures of 2.5 K. The thermal variation of the **a** unit-cell parameter is shown in Figure 9b. There is a change in the variation rate at about 100 K, and a peak at 25 K probably related to the Tb magnetic ordering; the observed singularity at ≈165 K is unrelated with any magnetic feature of this oxide.

Crystal Structure at 2 K. The structural refinement from the 2 K high-resolution NPD data (D2B instrument) was performed in the same way as the room-temperature analysis. The magnetic structure was introduced in the final refinement as a second phase; at 2 K it was necessary to introduce the

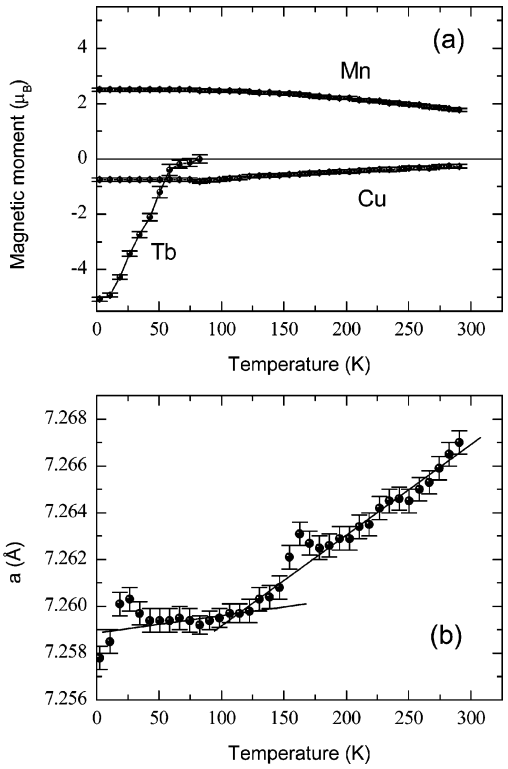

Figure 9. (a) Thermal variation of the ordered magnetic moments for Mn, Cu, and Tb determined from sequential NPD data. (b) Evolution of the cell parameter with temperature for $TbCu_3Mn_4O_{12}$ obtained from thermal evolution of NPD analysis; the straight lines are guides for the eye.

ordered Tb magnetic moments at 2a sites. The quality of the final fit is shown in Figure 5b and the relevant parameters are listed in Table 1 and Table 2. The discrepancy factors were $R_I = 6.36\%$ for the crystallographic phase and $R_I = 9.21\%$ for the magnetic one. The refined magnetic moments at 2 K are 2.59(7), −0.75(6), and −5.07(7) μ_B for Mn, Cu, and Tb, respectively. The ordered magnetic moment found at Mn positions is significantly lower than that expected for ($Mn_3^{4+}Mn^{3+}$) of 3.25 μ_B per atom, suggesting some electronic delocalization due to covalency effects.

Discussion

A view of the crystal structure of $TbCu_3Mn_4O_{12}$ is shown in Figure 10. This perovskite is fairly distorted due to the small size of Tb and Cu cations occupying the A positions of the structure, which force the MnO_6 octahedra to tilt in order to optimize the Tb−O and Cu−O bond distances. The tilting angle of the octahedra can be simply derived from the Mn−O−Mn angle, to be 19°. The cubic perovskite superstructure of $TbCu_3Mn_4O_{12}$ contains several features that must be highlighted. As is shown in Table 2, Tb atoms are coordinated to 12 oxygen atoms, with equal Tb−O distances of 2.435(2) Å at RT, while the oxygen environment for Cu^{2+} cations is highly irregular, with 8 rather long distances (2.75 and 3.19 Å at RT) and an effective coordination number of four, with Cu−O bond lengths of 1.952(2) Å at RT in a pseudo-square arrangement. These CuO_4 units are not strictly coplanar, exhibiting O−Cu−O angles of 94.0° and 86.0°. At the B substructure of the perovskite, (Mn^{4+}, Mn^{3+}) cations occupy the center of virtually regular octahedra, with Mn−O

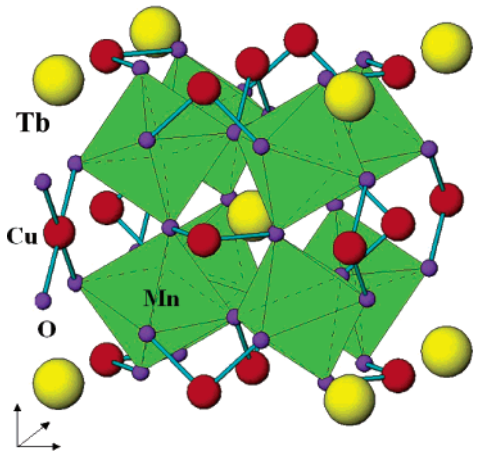

Figure 10. View of the structure of $TbCu_3Mn_4O_{12}$. **c** axis is vertical. Large, medium, and small spheres represent Tb, Cu, and O, respectively; corner-sharing MnO_6 octahedra are fairly tilted in the structure to optimize Tb−O and Cu−O bond lengths. It can be seen at the left the effective square planar coordination of Cu cations.

bond lengths of 1.922(1) Å at RT. From the chemical point of view, the presence of Tb cations replacing Ca^{2+} in $CaCu_3Mn_4O_{12}$ implies either the reduction of some Mn^{4+} cation to Mn^{3+} or the presence of some oxygen vacancies per formula unit. The last possibility was discarded by the neutron powder diffraction study. Also, the observed unit-cell parameter for the Tb perovskite, of 7.2668(1) Å, is considerably expanded with respect to that reported for the parent $CaCu_3Mn_4O_{12}$ oxide, of 7.241(1) Å,[9] which can also be seen as a result of the mentioned electronic injection.

The actual oxidation states of the different cations present in the solid can be assessed by means of the Brown's bond valence theory,[18,19] from the observed metal−oxygen distances. This theory gives a phenomenological relationship between the formal valence of a bond and the corresponding bond length. From the distances listed in Table 2, we obtain valences at RT of 3.23, 1.903, and 3.796 for Tb, Cu, and Mn, respectively. The valence of Tb cation was expected to be 3+ or 4+, and the result of the bond-valence study demonstrates it is closer to 3+. The valence for divalent Cu is slightly lower than expected. The valence for Mn at 8c (octahedral environment) is lower than 4+, and very close to the nominal valence of 3.75+ corresponding to a trivalent Tb nominal valence. This value corresponds to 75% of Mn^{4+} and 25% of Mn^{3+} at the B site. We can conclude that the incorporation of Tb^{3+} to the A positions of the perovskite involves the occurrence of a mixed Mn^{4+}−Mn^{3+} valence at the B sublattice. The electronic injection upon replacement of Ca by Tb is concomitant with the significant expansion of the unit-cell parameters, as described earlier. The Mn−O distance observed for $TbCu_3Mn_4O_{12}$, of 1.922(1) Å, is considerably longer than that observed for $CaCu_3Mn_4O_{12}$, of 1.915(1) Å,[9] consistent with the incorporation of larger Mn^{3+} cations in the Mn^{4+} sublattice. On the other hand, the Tb−O distance, 2.535(2) Å, is smaller than the Ca−O one, 2.56 Å, in the parent compound,[9] due to the smaller ionic

(18) Brown, I. D. *Structure and Bonding in Crystals*; O'Keefe, M., Navrotsky, A., Eds.: Academic Press: New York, 1981; Vol. 2, pp 1−30.
(19) Brese, N. E.; O'Keefe, M. *Acta Crystallogr. Sect. B* **1991**, *47*, 192.

radius of Tb^{3+}, 1.04 Å in 8-fold coordination,[20] compared with that of Ca^{2+} (1.12 Å).

$TbCu_3Mn_4O_{12}$ is a ferrimagnet with $T_C = 395$ K; there is an increment of T_C with respect to the parent $CaCu_3Mn_4O_{12}$ oxide ($T_C = 355$ K),[3] which might be a result of the electronic injection upon Ca^{2+} replacement by Tb^{3+}, reinforcing the superexchange interactions between Mn cations, perhaps as a result of a carrier-mediated exchange mechanism which is triggered at the Mn sublattice via induction of a mixed valence for Mn. In the same direction, the electronic injection is also patent in the transport properties of this perovskite, where a low resistivity and a metallic behavior is observed, in sharp contrast with the insulating (semiconducting) character reported for the parent Ca-containing oxide. The MR is always negative and increases with decreasing temperature (inset of Figure 4); a maximum value of 25% is achieved under $H = 9$ T. In $CaCu_3Mn_4O_{12}$ compound, MR is around 40%.

In the temperature interval between T_C (395 K) and about 100 K, the magnetic structure can be described as a perfect ferrimagnetic arrangement of Mn and Cu spins, as demonstrated from NPD data. Tb magnetic moments are paramagnetic, i.e., are not long-range ordered in this intermediate temperature regime. The expected saturation magnetic moment in this temperature range would be around 10 μ_B/f.u., for the stoichiometry $Tb^{3+}Cu_3^{2+}(Mn_3^{4+}Mn^{3+})_BO_{12}$ (Cu^{2+}, $S = {}^1/_2$; Mn^{3+}, $S = 2$; Mn^{4+}, $S = {}^3/_2$). This value is roughly the one experimentally reached at 100 K under $H = 16$ T (Figure 3b). The low-temperature magnetic structure involves, below 100 K, the participation of Tb magnetic moments in the long-range ordered magnetic arrangement, as depicted in Figure 8b. It seems that this configuration is not particularly stable since it can be destroyed upon the application of a relatively low external magnetic field. As shown in the magnetization vs field isotherms below $T = 100$ K, there is a monotonic evolution of the magnetization above small threshold fields of 0.2 T, which can be explained as a progressive turning-over of the Tb magnetic moments from the orientation adopted in the magnetic structure stable at $H = 0$, illustrated in Figure 8b, to the situation schematized in Figure 8c, where the Tb moments are aligned to the Mn spins. Under the highest external magnetic fields of 16 T, the maximum reached magnetization at 2 K overcomes 15 μ_B/f.u., implying that an extra magnetization of about 5 μ_B/f.u. corresponds to Tb magnetic moments aligned parallel to the Mn spins. This picture, based on magnetization measurements, must be verified by neutron diffraction experiments under a magnetic field.

(20) Shannon, R. D. *Acta Crystallogr. A* **1976**, *32*, 751.

Conclusions

Single-phase $TbCu_3Mn_4O_{12}$ with a perovskite-related structure was synthesized at a moderate pressure of 2 GPa in the presence of an oxidizing agent. The crystal structure was refined at RT and 2 K from high-resolution NPD data; a bond valence study demostrates that Tb adopts a trivalent oxidation state, despite the strongly oxidizing synthesis conditions, and Mn presents a mixed valence state close to the expected $Mn^{3.75+}$. $TbCu_3Mn_4O_{12}$ is a ferrimagnet with $T_C = 395$ K; there is an increment of T_C with respect to the parent $CaCu_3Mn_4O_{12}$ oxide, which is thought to be a result of the electronic injection upon Ca^{2+} replacement by Tb^{3+}, inducing a mixed valence state at the Mn sublattice and reinforcing the superexchange interactions between Mn cations. Additionally, this electronic injection is also responsible for a lower resistiviy and metallic behavior, as well as a reduced magnetoresistance. The microscopic origin of the magnetic behavior in this material at $H = 0$ has also been unraveled from NPD data. Below T_C and down to 100 K, the magnetic structure can be defined as a ferrimagnetic (antiparallel) aligment of Mn and Cu spins; below 100 K the Tb magnetic moments participate in the long-range magnetic ordering, exhibiting an antiferromagnetic coupling to the Mn magnetic moments. The Tb magnetic coupling can be broken under the application of external magnetic fields, inducing a turnover of the Tb moments which then become parallel to the Mn spins. This point needs to be verified in a neutron experiment performed under magnetic field.

Acknowledgment. We are thankful for the financial support of CICyT for the projects MAT2004-0479 and MAT2003-01880 and of the CAM for the projects GR/MAT/0427/2004 and GR/ MAT/0771/2004, and we are grateful to ILL for making all facilities available.

CM051265L